Thermally evaporated Cu-Co top spin valve with random exchange bias

Thermally evaporated Cu–Co top spin valve with random exchange bias

Alessandro Chiolerio, Paolo Allia, Angelica Chiodoni, Fabrizio Pirri, Federica Celegato et al.

Citation: J. Appl. Phys. **101**, 123915 (2007); doi: 10.1063/1.2749289
View online: http://dx.doi.org/10.1063/1.2749289
View Table of Contents: http://jap.aip.org/resource/1/JAPIAU/v101/i12
Published by the American Institute of Physics.

Thermally evaporated Cu–Co top spin valve with random exchange bias

Alessandro Chiolerio, Paolo Allia,[a] Angelica Chiodoni, and Fabrizio Pirri
Physics Department, Politecnico di Torino, Corso Duca degli Abruzzi 24, I-10129 Turin, Italy

Federica Celegato and Marco Coïsson
Istituto Nazionale di Ricerca Metrologica, Strada delle Cacce 91, I-10135 Turin, Italy

(Received 5 October 2006; accepted 10 May 2007; published online 25 June 2007)

A cobalt-copper top spin valve was prepared by thermal evaporation of a stack of ferromagnetic thin films separated by thin layers of the diamagnetic metal, with a cap layer containing an antiferromagnetic (AFM) exchange-biasing material. A nonconventional top AFM layer was used, in order to optimize the multilayer roughness and to avoid electrical interference with metallic layers; it consists of a composite material easily processed by means of optical lithography, basically a polymeric matrix composite with a dispersion of nickel oxide microparticles. Magnetization and magnetoresistance measurements were performed from 4 to 300 K. The measurements of both quantities indicate random pinning action of the top AFM layer, resulting in a small exchange-bias field and in asymmetric magnetization and magnetoresistance curves. A simple model explains the observed physical effects. © *2007 American Institute of Physics*. [DOI: 10.1063/1.2749289]

I. INTRODUCTION

Since their discovery, spintronic effects in metallic systems and related spintronic devices have attracted the attention of researchers because of interesting physical effects and applications.[1,2] One of the simplest and most popular spintronic devices not involving semiconductors is the spin valve,[3] based on the basic stacking FM/NM/FM, where FM is a ferromagnetic metal or alloy, and NM is a nonmagnetic metal; interlayer exchange coupling (IEC) provides stability for either parallel (P) or antiparallel (AP) magnetization configuration in the two FM layers, depending on the thickness of the NM spacer.[4] The ensuing giant magnetoresistance (GMR) effect[5–8] allows one to determine the magnetic configuration of the device monitoring its electrical resistance. The magnetization of one of the two FM films may be pinned by means of exchange coupling[9,10] (EC) provided by an additional layer of antiferromagnetic (AFM) material such as NiO; that of the free layer may be easily varied by an external magnetic field.[11] The roughness of surfaces and interfaces plays a central role when the response of the spin valve is to be optimized for applications;[12] a low roughness also provides an efficient exchange coupling between the AFM material and the adjacent FM layer.[13] In this work, spin valves of the family $(Co_x/Cu_y)^n/NiO$, where the subscript indicates the film thickness in angstroms and the superscript indicates the number of repetitions, were prepared by means of thermal evaporation (TE) on monocrystalline silicon substrates, in order to test this cheap manufacturing technique.[14] AFM NiO layers obtained by high temperature thermal oxidation of nickel films usually exhibit a strong intrinsic roughness which may be detrimental both to an efficient exchange coupling and to the interfacial spin dependent scattering, when the spin-valve structure mimics the underlying NiO roughness because of conformal growth. In this work, an alternative method to provide exchange bias was attempted by exploiting a NiO micropowder dispersed into a polymeric matrix and placed on top of the structure. This material is characterized by a high thermomechanical stability from the liquid helium region up to temperatures exceeding 500 K. It is easily processed by means of optical lithography, and basically consists of a photosensitive polymeric matrix composite (PMC) with a dispersion of nickel oxide microparticles. Other solutions explored for the top AFM layer integration are based on sputter deposition of a biasing material;[13] in the present case we experimented the application of low temperature synthesized powders, whose inclusion in a multilayered structure necessarily requires a hard-enable mechanical support, in this case a thermoset resin.

II. EXPERIMENT

A high-vacuum TE system was exploited to evaporate thin films of cobalt and copper, starting from very pure (>99.95%) raw materials; the multilayer was produced *in situ* on single side polished Si(100) wafers, after cleaning cycles in organic solvents to remove grease and dust from the surface and improve adhesion, and in HF solution to remove native oxide and therefore stabilize the low-anisotropy fcc phase of Co against the hcp one [as confirmed by x-ray diffraction (XRD) analysis]. The evaporation took place at room temperature (RT), with a base pressure of 4×10^{-8} Torr; the film thickness was monitored by a resonant crystal thickness monitor and checked *ex situ* by a profilometer and high resolution electronic imaging on a section of the material. The resulting stack was $Si/Co_{40}/(Cu_{18}Co_{35})$.[8] A nickel oxide micrometer-sized powder was obtained by low temperature thermal decomposition of nickel hydroxide in air (650 K); its chemical purity and crystal structure were checked by XRD spectra. The layer containing the AFM oxide was prepared by mixing the polymeric component (a liquid novolak) with the solid machined NiO powder; it was deposited on top of the multilayer and cured in a vacuum

[a]Electronic mail: paolo.allia@polito.it

oven at 400 K. The importance of keeping clean interfaces between NiO and Co led us to a careful control of the curing time, during which the particles were allowed to precipitate, driven by gravity. In order to set a magnetic anisotropy with easy axis coincident with the direction chosen for the electrical current flow, the structure was field annealed (FA) from above the Néel temperature of NiO (528 K) down to room temperature under a static external magnetic field of about 1 kOe.

The structure and morphology of the prepared sample were studied by using a ZEISS SUPRA™ 40 field emission scanning electron microscope (FESEM); this imaging instrument has an extremely low magnetic field outside the objective lens, thus enabling investigation of magnetic materials and devices. A field emission cathode in the electron gun provides narrower probing beams at low as well as high electron energies, resulting in both improved spatial resolution and minimized sample charging and damage.

Magnetization measurements were performed by means of an alternating-gradient force magnetometer (AGFM), taking into account the true values of film area and film thickness in order to evaluate the sample magnetization. The applied field was parallel to the film plane, and the measurements were performed from 5 to 300 K up to 18 kOe. At each temperature, three magnetic signals were systematically detected by performing subsequent temperature runs: (a) the overall signal from the whole sample, (b) that from the clean substrate, and (c) that from the empty AGFM sample holder and probe. A numeric algorithm was employed in order to remove both high order harmonics and magnetic signals provided by the substrate and the AGFM probe, making use of the finite impulse response (FIR) filtering functions.

Magnetotransport measurements were made by means of the four-contact technique[15] using thick copper Ohmic contacts directly evaporated on the structure through a metallic mask, and indium solders to reduce the amount of heat transferred to the multilayer during soldering operations. The magnetoresistance data were collected at fixed temperatures in the same range (5–300 K) up to 70 kOe. The magnetic field was in plane and parallel to the electrical current flow.

III. RESULT AND DISCUSSION

A. Structure and morphology of the TSV

FESEM analysis provides information about the adhesion between the cap layer and the metallic stacking and about the general layout of the structure. A region where the macroscopic composite cap layer has been removed through mechanical friction is shown in Fig. 1. Three different depth levels are observed, the bottommost corresponding to the silicon substrate, the middle one to the magnetic multilayer, and the topmost to a thin sheet of polymeric matrix containing NiO microparticles. In order to image this sectionlike portion, the specimen holding stage was tilted of 37° out of plane; the tilting correction factor for measured features, derived from simple geometrical considerations, leads to a total thickness of 44 nm for the metallic stacking and of 36 nm for the polymer cap. The latter has a smooth appearance and also a greater contrast with respect to the other materials of the specimen, because of both low conductivity and great amount of charge trapped on its surface. The presence of a non-negligible fraction of the original polymeric cover after strong friction treatment also demonstrates the existence of a great mechanical grip between evaporated metal and cured thermoset resin.

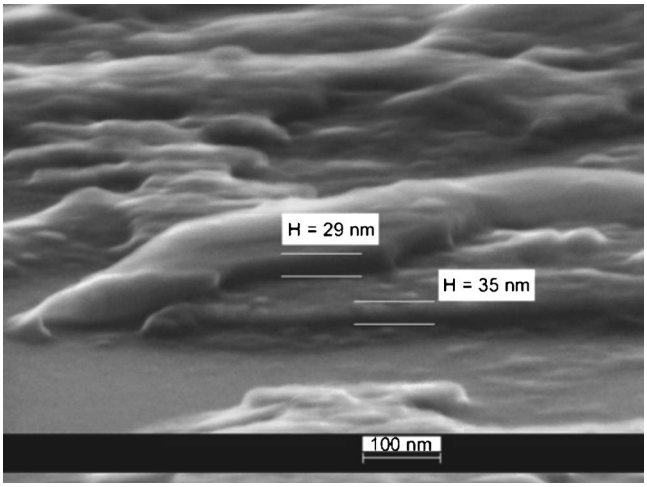

FIG. 1. SEM image of the surface of the TSV showing the contact area between the polymeric cap layer (smooth in the top) and the metallic stacking (darker below) evaporated on monocrystalline silicon, in a region previously subjected to abrasion. Apparent thicknesses of both layers are shown. Magnification 450 000×.

B. Magnetic measurements

The magnetization of the top spin value (TSV) is shown in Fig. 2(a) at two representative temperatures after subtraction of all spurious effects. The magnetization always shows a strongly unsaturating behavior with an almost linear dependence on H at high fields; this may indicate a substantial contribution from magnetically frustrated regions,[16] which may exist in the whole multilayer volume. In order to explain the high-field features of Fig. 2(a), magnetization measurements (not shown here) were performed as functions of temperature on a sample of isolated NiO-containing resin. They reveal a ferromagnetic response (>900 Oe coercivity at T =100 K) with loop asymmetry (bias field: 120 Oe at T =100 K, disappearing above 200 K) and unsaturating tails. Ferromagneticlike behavior in low temperature synthesized NiO nanocrystalline materials was previously found[17] and explained as the simultaneous effect of missing bonds and lattice stress; the chemical synthesis in our case may lead to nanometer-scale precipitates that coalesce during thermal decomposition forming larger (micrometer-sized) aggregates. We estimated from the volume ratio of NiO that at 100 K and 18 kOe the net magnetic moment contribution of NiO in our TSV exceeds 60% of the total measured moment, while at 300 K this contribution drops to 40%. The ferromagnetic response of granular NiO does not entirely explain the unsaturating behavior of magnetization curves [Fig. 2(a)]. Starting from the known high-field magnetic contribution of

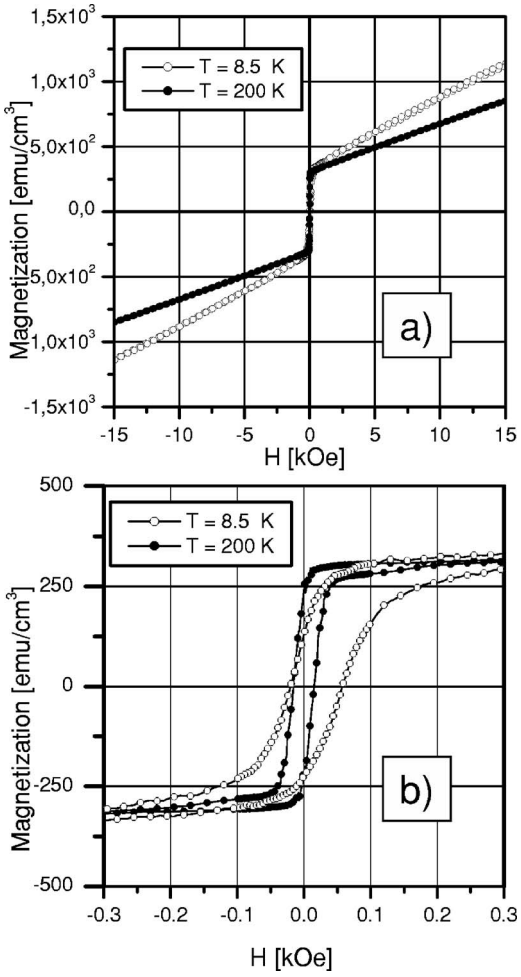

FIG. 2. Hysteresis loops of the TSV measured at 8.5 and 200 K and depurated from spurious effects (open and full circles, respectively), shown in the whole magnetic field range (a) and at low fields (b).

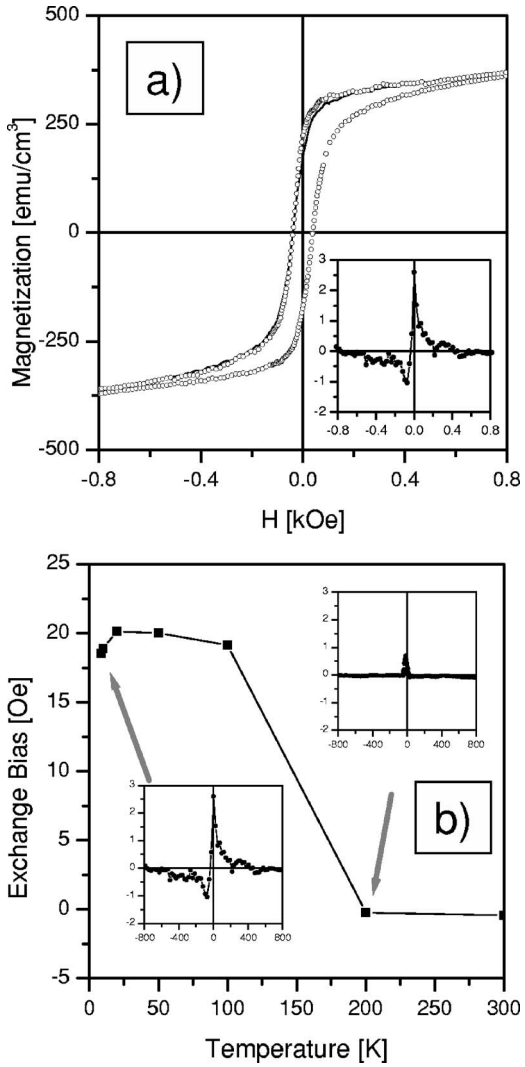

FIG. 3. (a) Hysteresis loop at 8.5 K (circles). Full line: complete reflection of the lower branch with respect to the origin. Inset: difference between experimental upper branch and lower-branch reflection, showing an anomalous behavior at low fields. (b) Exchange-bias field measured at various temperatures. The insets report the asymmetry of the hysteresis loop.

NiO and considering that fcc Co saturates well below 1 kOe, it was possible to estimate that the volume fraction of frustrated Co over total metal was about 50%.

When the low-field region of the hysteresis loops is analyzed in more detail [Fig. 2(b)], a slight asymmetry is observed: The magnetization curve measured under decreasing fields (above) does not exactly correspond to total inversion with respect to the origin of the corresponding curve measured under increasing fields (below). This is shown in Fig. 3(a), referring to $T=8.5$ K, where the curve obtained by total inversion of the bottom branch is reported as a full line. The upper branch exhibits a slower decay at remanence and a faster change around coercivity with respect to the full line, as shown in the differential plot in the inset of Fig. 3(a). This behavior is believed to originate from the exchange-bias effect of the AFM material; the anomaly decreases with increasing temperature and disappears above 200 K. The exchange-bias field H_{bias} (defined as the difference between absolute coercivities of each loop) is reported in Fig. 3(b). This quantity is rather small (maximum $H_{\text{bias}}=20$ Oe at low temperatures) and disappears before 200 K, i.e., at temperatures well below those usually found in biased systems of the same type.[18] Exchang-bias values up to 120 Oe can be obtained in spin valves containing continuous NiO layers after proper annealing and careful control of interface quality.[13] A comparison between Figs. 2 and 3(b) confirms that the loop asymmetry of the TSV scales with the exchange-bias field. The initial susceptibility at the two coercive fields (measured as the slope of the experimental M vs H curves) shows again an asymmetric behavior of the half loops which merge above 200 K (Fig. 4). Another possible explanation of the biasing effect may be found in the presence of CoO located at the interface between the topmost Co layer and the NiO-dispersed resin; in fact, we cannot exclude a partial oxidation, yet we believe that this nonstandard behavior is related to the anomalous NiO whose relative contribution on the TSV magnetization is rather high.

The TSV exhibits a complex magnetoresistive response at low temperatures, as shown in Fig. 5. No "giant" effects were observed, the maximum magnetoresistance (MR) being of the order of 0.6% at 5 K. The measured MR is clearly not monotonic and unsymmetrical. With reference to Fig. 6, the three main features observed in this TSV are as follows: a low-field dip occurring up to about 350 Oe (labeled "A");

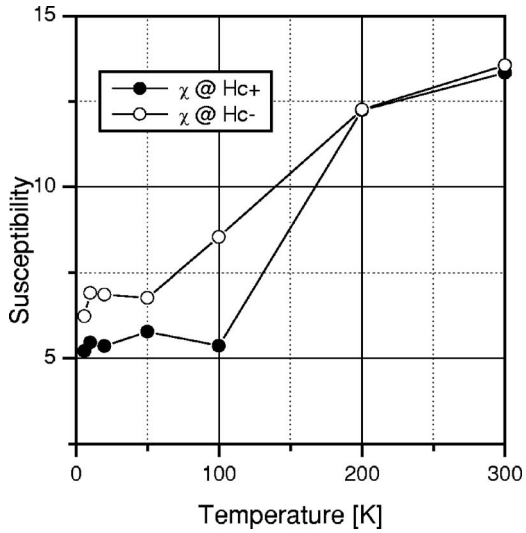

FIG. 4. Magnetic susceptibility (measured at the coercive fields) as a function of temperature.

the asymmetry of the magnetoresistive response, whose peak values depend on the magnetic history of the sample ("B"); and the unsaturating negative MR at high fields ("C"). The low-field dip is related to anisotropic magnetoresistance (AMR), which is basically related to field-induced reorientation of wave function orbitals with respect to the electrical current direction.[19] The simultaneous presence of AMR and GMR has been observed in other layered systems.[20] The negative, unsaturating MR measured at high fields is instead explained as GMR, indicating the presence of magnetically frustrated regions, where the spins are noncollinear down to distances of the order of the electronic mean free path. MR results, strictly originating from the metal layers with the exclusion of the NiO-resin cap layer, confirm our previous indication that the high-field linear slope of Fig. 2(a) is not only due to NiO anomalous behavior but also to frustrated Co.

C. Model

The observed effects can be explained by a simple model of this TSV. All layers of the FM/NM/FM stacking are characterized by a small roughness related to the preparation technique, which can be quantified from morphologic analysis based on atomic force microscopy as a rms roughness <1 nm for thin films directly evaporated on polished silicon wafers. By comparison, TE films on thermally synthesized NiO films in the bottom SV architecture are typically affected by a much higher roughness, of about 8 nm. However, the FM layer in contact with the polymer is submitted to an exchange anisotropy effect of randomly variable direction and strength induced by the NiO microparticles in atomic contact with the Co layer, whose size and crystallographic orientation are randomly distributed. As a consequence, the FM layer is composed of small regions whose magnetization is randomly pinned by NiO particles embedded in the polymer matrix; the exchange biasing efficiency depends on the ratio between Co/particle surface contact area and the whole FM cap layer surface. As a consequence, the local anisotropy for the magnetization in the adjacent FM layer is distributed in magnitude and direction, and may also be oriented significantly out of the TSV plane. Although the FM layer closest to the AFM capping is influenced most by random pinning, it is likely that the effect propagates to some extent to other Co layers in the stack via magnetic interaction mediated by the Cu interlayers.

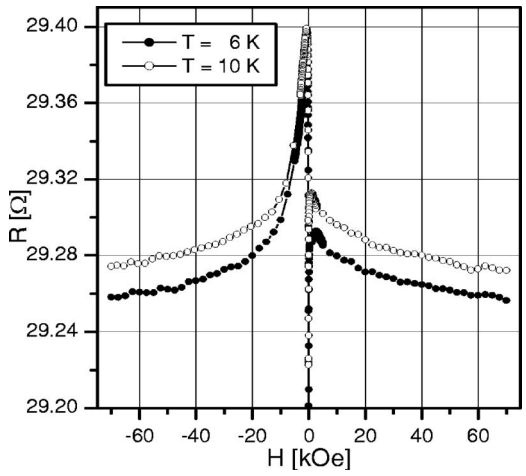

FIG. 5. Magnetoresistance curves at 6 and 10 K.

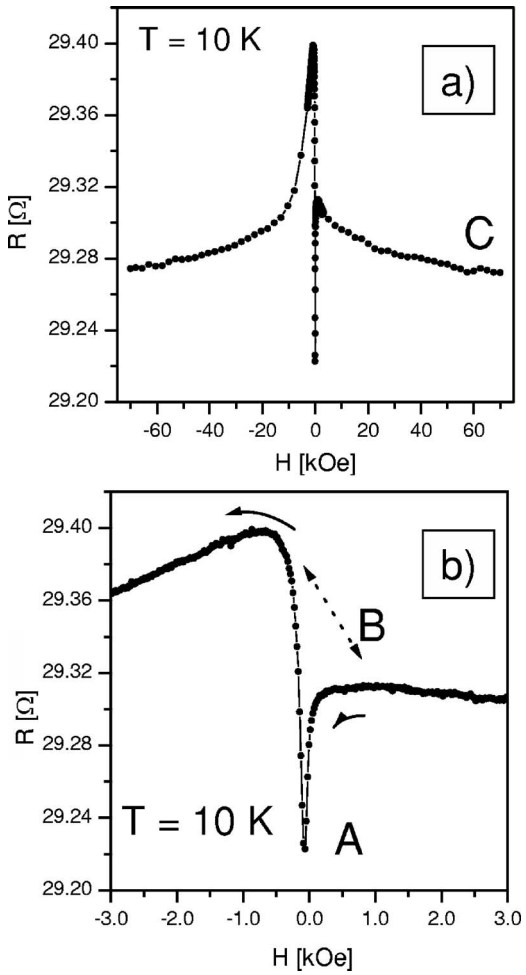

FIG. 6. Magnetoresistance at 10 K, in the whole range of external field (a) and in the low-field region (b). The low-field dip is labeled as "A," the asymmetry of the resistance peak depending on the history of external field is labeled as "B," and the slowly saturating tails are labeled as "C."

Considering completely random pinning directions, we should obtain no macroscopic biasing effect at all. Let us consider three leading magnetic energy terms in the standard planar model,[9,21]

$$E = -M_s H \cos\vartheta + K_u \sin^2\vartheta + \tilde{K}\cos(\vartheta - \alpha), \tag{1}$$

where M_s is the saturation magnetization, K_u is the leading magnetic anisotropy constant (whose easy axis is supposed directed as the applied field), $\tilde{K}$ is the exchange-bias anisotropy constant, and α is the (random) angle between the local pinning axis and the direction of the applied field. If the mean value $\langle\cos(\vartheta-\alpha)\rangle$ is evaluated for a uniform distribution of α from 0 to 2π, $\langle\cos(\vartheta-\alpha)\rangle=0$, so that there is no net bias field,

$$H_{\text{bias}} = \frac{\tilde{K}\langle\cos\alpha\rangle}{M_s} \equiv 0. \tag{2}$$

However, a biasing effect survives, related to the rms energy term

$$E_p = \tilde{K}\langle\cos^2(\vartheta-\alpha)\rangle^{1/2}, \tag{3}$$

where $\langle\cos^2(\vartheta-\alpha)\rangle=\cos^2\vartheta\langle\cos^2\alpha\rangle+\sin^2\vartheta\langle\sin^2\alpha\rangle+\cos\vartheta\sin\vartheta\langle\sin 2\alpha\rangle=1/2$, so that the pinning energy density is just $E_p=2^{-1/2}\tilde{K}$.

Although random pinning does not provide a net exchange-bias field, it should bring about detectable effects on magnetization (and magnetotransport) properties of the pinned material. As a matter of fact, the pinning directions in our TSV are not completely random, owing to the field-cooling treatment with the external field axis in plane parallel to the prospective direction of electrical current flow, which provides a source of anisotropy for the distribution of the local pinning directions. If the pinning direction $\alpha=0$ $(\equiv 2\pi)$ is privileged with respect to $\alpha=\pi$, $\langle\cos\alpha\rangle$ is nonzero and a weak bias field appears, as indeed observed in Fig. 3(b). As a consequence, it is assumed that the spin structure of the FM layer in contact with the polymer consists of submicrometric, coherent zones—determined by the random pinning—whose spacing is of the same order of magnitude of the electron mfp (see Fig. 7). The transition from one region to another is marked by competing magnetic interactions giving rise to local frustration and micromagnetic states, even though the spin alignment is not completely random due to strong exchange interactions. We refer to these transition regions as "shells" surrounding each coherent-magnetization region (or "core"). Magnetically ordered cores and disordered shells are often found in certain nanoparticle systems.[22]

The bold arrows in Fig. 7 indicate the core magnetization; the dashed arrows indicate the local magnetization in shells, which gradually aligns according to the core orientation as the core-shell boundary is approached. The double arrows indicate the projection on the plane of the local random anisotropy direction; the shorter the arrow, the greater the component that lies out of plane. Let us start with the sample close to magnetic saturation in one direction [H

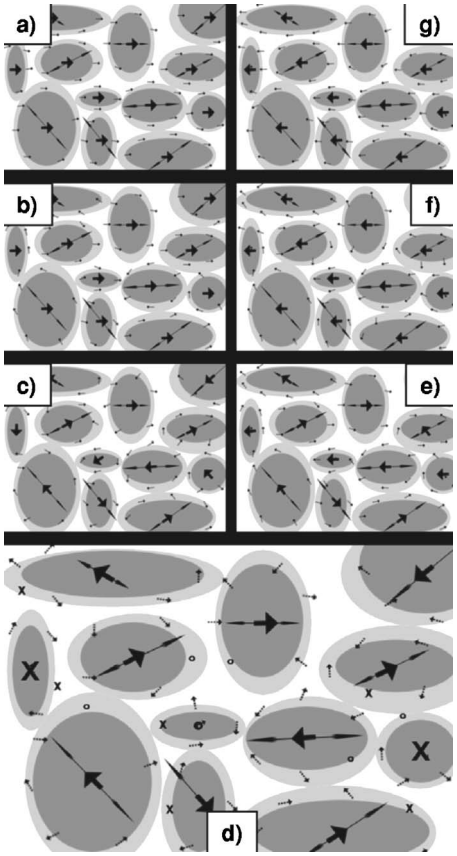

FIG. 7. A sketch of the proposed spin structure of thermally evaporated TSV. Pinned cores and transition shells are pictured in dark and light gray, respectively. (a) Almost complete positive saturation, $H\cong 70$ kOe; (b) intermediate field, $H\cong 30$ kOe; (c) $H\cong 350$ Oe; (d) zero field; (e) $H\cong -350$ Oe; (f) $H\cong -30$ kOe and (g) $H\cong -70$ kOe.

$\cong 70$ kOe, Fig. 7(a)]. When the field is being reduced to zero, but is much larger than a field $\tilde{H}$ defined as

$$\tilde{H} \approx \frac{E_p}{M_s} = \frac{2^{-1/2}\tilde{K}}{M_s}, \tag{4}$$

the core magnetization is still basically aligned with the field, while the magnetization in shells rapidly loses the field-induced alignment [$H\cong 30$ kOe, Fig. 7(b)]. The increasing misalignment of M in adjacent shells is responsible for the almost linear behavior of isothermal magnetization at high fields (Fig. 2), and is the origin of the measured increase in the sample's electrical resistance (which is mostly an interfacial effect, i.e., one which originates within and between the shells). When the external field becomes comparable to or lower than the rms pinning field, the core magnetization starts to follow the local easy axis, while the shell magnetization is highly disordered [$H\cong 350$ Oe, Fig. 7(c)]. A similar picture holds for $H\cong 0$ [Fig. 7(d)], where the disorder of both core and shell magnetization directions is a maximum. Now, the dispersion of core magnetization directions below $\tilde{H}$ obviously affects the overall magnetization without having a dramatic effect on the GMR, dominated by interface (intershell) scattering. However, a fraction of the core magnetization now points at high angles with respect to the film plane (and to the electrical current direction), as sketched in

Fig. 7(d). As a consequence, an AMR effect develops in cores whose magnetization is perpendicular to the TSV plane. It should be reminded that the AMR is a bulk effect,[20] and that the cores have sizes great enough to fulfill this condition. This is the origin of the resistance dip, which is observed when $|H| < \tilde{H} \cong 350$ kOe (Fig. 6). Using $M_s \cong 1400$ emu/cm^3, the value of $\tilde{K}$ turns out to be 6.9×10^5 ergs/cm^3. The bias field H_{bias} is instead as small as 20 Oe at low temperatures [Fig. 3(b)]. Using Eqs. (2) and (4), one gets $\langle \cos \alpha \rangle \cong 0.04$: The field-cooling treatment of the polymeric composite is not particularly efficient in inducing a preferential biasing direction.

When the magnetic field is inverted, the AMR resistive dip disappears [$H \cong -350$ Oe, Fig. 7(e)]; for higher $|H|$ values, spin reversal occurs in some cores, thus generating an additional magnetic disorder in the spin transition regions that separate the antiparallel core magnetizations; the electrical resistance therefore attains values higher than previously reached, resulting in the observed MR asymmetry (feature B in Fig. 6). For still higher $|H|$ the micromagnetic shell magnetization gradually aligns to the field direction [Figs. 7(f) and 7(g)], giving rise again to an unsaturating GMR.

IV. CONCLUSIONS

A thermally evaporated TSV of the family Si/Co/$(\text{Cu/Co})^n$/NiO was produced and characterized. Thermal evaporation (TE) was chosen as the deposition technique for its versatility and low costs beneficial to prospective application. The top architecture was chosen to improve interfacial roughness and the AFM material (NiO micropowder) was mechanically blocked in a cured photosensitive resin, in order to exploit the advantages of an easy optical lithography process and of a great thermomechanical stability.

Magnetic measurements under in-plane magnetic field indicate that the sample cannot be easily saturated at any temperature, exhibiting a high-field behavior reminiscent of a highly disordered magnetic phase. This is partly ascribed to an anomalous behavior found in the low temperature synthesized NiO powder, which revealed a ferromagnetic response, bias field, and unsaturating tails; partly to frustrated Co regions, whose amount was estimated to be approximately 50% in volume of total Co.

Magnetotransport properties indicate that standard GMR is not the main effect in this TSV, presumably because of an unavoidable interlayer roughness, inherent to the production process. Instead, a complex, strongly asymmetric behavior of the electrical resistance including AMR and GMR is observed.

Magnetic and magnetotransport properties suggested us a core-shell picture of the spin structure, where core regions of one or more Co layers experience a local anisotropy and a pinning field provided by AFM particles, while magnetically disordered regions wrapping the cores exhibit a micromagnetic state. This model explains the strong asymmetry observed in magnetoresistance curves and the weaker asymmetry of magnetization loops, as well as the unsaturating character of both magnetization and magnetoresistance at high fields.

It is concluded that the use of thermal evaporation in conjunction with thermal curing of a NiO-dispersed PMC is effective in preparing spin valves with a very low cost and short processing time. However, the quite high roughness of thermally evaporated thin films is detrimental to interface planarity, and this should be taken into account when the working principle of the device is based on interfacial scattering. The anomalous behavior of NiO resulted in a variety of different effects, as the high-field unsaturating magnetization and ferromagneticlike response, which need to be limited. Furthermore, the biasing effect here analyzed involves mostly the topmost Co layer and only in smaller amount the other deeper layers, whose effect is the multiplication of rough interfaces and frustrated regions. Future studies will analyze the relationship between NiO crystal size and ferromagnetism, in order to optimize the low temperature synthesis process and the AFM characteristics.

[1] I. Zutic, J. Fabian, and S. Das Sarma, Rev. Mod. Phys.. **76**, 323 (2004).
[2] M. Ziese and M. J. Thornton, *Spin Electronics* (Springer, Berlin, 2001), p. 10.
[3] B. Dieny, J. Appl. Phys. **69**, 4774 (1991).
[4] P. J. H. Bloemen, R. van Dalen, W. J. M. de Jonge, M. T. Johnson, and J. aan de Stegge, J. Appl. Phys. **73**, 5972 (1993).
[5] J. M. Daughton, J. Magn. Magn. Mater. **192**, 334 (1999).
[6] M. N. Baibich, J. M. Broto, A. Fert, F. Nguyen Van Dau, F. Petroff, P. Etienne, G. Creuzet, A. Friederich, and J. Chazelas, Phys. Rev. Lett. **61**, 2472 (1988).
[7] R. E. Camley and J. Barnas, Phys. Rev. Lett. **63**, 664 (1989).
[8] S. S. P. Parkin, N. More, and K. P. Roche, Phys. Rev. Lett. **64**, 2304 (1990).
[9] W. H. Meiklejohn and C. P. Bean, Phys. Rev. **105**, 904 (1957).
[10] A. E. Berkowitz and R. Takano, J. Magn. Magn. Mater. **200**, 552 (1999).
[11] H. D. Chopra, B. J. Hockey, P. J. Chen, W. F. Egelhoff, Jr., M. Wuttig, and S. Z. Hua, Phys. Rev. B **55**, 8390 (1971).
[12] W. F. Egelhoff, Jr., P. J. Chen, C. J. Powell, R. D. McMichael, and M. D. Stiles, Prog. Surf. Sci. **67**, 355 (2001).
[13] D. G. Hwang, C. M. Park, and S. S. Lee, J. Magn. Magn. Mater. **186**, 265 (1998).
[14] K. Matsuyama, H. Asada, S. Ikeda, K. Umezu, and K. Taniguchi, IEEE Trans. Magn. **32**, 3612 (1996).
[15] S. Tumanski, *Thin Film Magnetoresistive Sensors* (Institute of Physics, Bristol/Taylor & Francis, London, 2001), p. 208.
[16] P. Allia, M. Coisson, J. Moya, V. Selvaggini, P. Tiberto, and F. Vinai, Phys. Rev. B **67**, 174412 (2003).
[17] H. Bi, S. Li, Y. Zhang, and Y. Du, J. Magn. Magn. Mater. **277**, 363 (2003).
[18] A. J. Devasahayam and M. H. Kryder, IEEE Trans. Magn. **35**, 649 (1999).
[19] T. R. McGuire and R. I. Potter, IEEE Trans. Magn. **4**, 1018 (1975).
[20] V. Franco, X. Battle, and A. Labarta, J. Appl. Phys. **85**, 7328 (1999).
[21] E. C. Stoner and E. P. Wohlfarth, Philos. Trans. R. Soc. London, Ser. A **240**, 599 (1948).
[22] L. Savini *et al.*, J. Appl. Phys. **91**, 8593 (2002).